Transactions of the Materials Research Society of Japan 28 [3] 655-658 (2003)

Fatigue Crack Propagation Behavior in TiNi Shape-Memory Alloys

Hidehiko Kimura, Keisuke Tanaka, Yoshiaki Akiniwa and Yuya Yoshida*
Nagoya University, Furo-cho, Chikusa-ku, Nagoya, 464-8603, Japan
Fax: 81-52-789-3109, e-mail: h_kimura@mech.nagoya-u.ac.jp
* Graduate School of Nagoya University, Furo-cho, Chikusa-ku, Nagoya, 464-8603, Japan
Fax: 81-52-789-3109

An experimental study was conducted on the room-temperature fatigue crack propagation behavior of two types of TiNi shape-memory alloy, FML4 that exhibits shape-memory effect at room temperature with the martensitic transformation start temperature M_s = 21 ℃ and superelastic FML6 with the reverse transformation finish temperature A_f = -20 ℃ . The single-edge-notched specimens were fatigued under cyclic axial tension compression with the stress ratio of R = -1 in air. The results show that the crack propagation rate in FML4 is smaller than that in FML6 when compared at the same stress intensity range. The threshold value of the stress intensity range is larger in FML4. The crystallographic orientation analysis by EBSP shows that most of grain boundaries in FML6 are high angle grain boundaries. Based on the observation of fatigue crack propagation behavior on the specimen surface by SEM and EBSP after fatigue test in FML6, branched cracks are found to be arrested at high angle grain boundaries, indicating that crack propagation resistance is increased owing to the grain boundaries in austenitic phase.

Key words: TiNi alloy, Shape-Memory Alloy, Fagitue, Crack Propagation, EBSP

1. INTRODUCTION

Shape memory alloy TiNi has been utilized for practical applications such as pipe joints and spectacle frames because of the stable shape-memory effect and advantages in mechanical properties, workability, corrosion resistance and biocompatibility. In recent years, TiNi alloys have been expected for the usage as the actuator of intelligent materials and structures. In order to utilize TiNi alloys as actuators, the fatigue property must be clarified to ensure the reliability of the materials and structures. However, the number of the study on the fatigue crack propagation behavior[1] is limited and the mechanism that governs the fatigue life of TiNi alloys, especially the effect of microstructure and the influence of the martensitic phase, is not fully understood.

In this study, fatigue crack propagation behavior of TiNi was investigated. The results of shape-memory TiNi and superelastic TiNi were compared and the microstructural effect on the crack propagation behavior was investigated.

2. EXPERIMENTAL PROCEDURES

2.1 Material and specimen

Two types of TiNi shape-memory alloy, KIOKALLOY manufactured by Daido Steel Co., Ltd., were utilized in this study: FML4 that exhibits shape-memory effect and superelastic FML6 at room temperature. The martensitic transformation finish temperature M_f, martensitic transformation start temperature M_s, reverse transformation start temperature A_s and reverse transformation finish temperature A_f are shown in Table 1. The scanning electron micrographs of the electrolytically polished specimen surfaces followed by etching are shown in Fig. 1. The grain size measured by the image data processing on the specimen surface is presented in Table 2. The grain sizes d_L and d_R correspond to the average grain length in the axial and radial direction of the round bars, respectively. The grains in the both specimens are slightly elongated in the axial direction. The grain size d_{eq} is the equivalent diameter. Figure 2 shows the dimensions of single-edge-notched specimens prepared from the round bars with the axial direction parallel to the loading axis by electrical discharge machining. The specimen surfaces were finished by electrolytic polishing after diamond paste and emery paper grinding.

2.2 Test condition

Fatigue tests were conducted under cyclic axial loading with the stress ratio R = -1 in air at room temperature. Crack length was measured by optical microscopes and crack opening load was measured by the unloading elastic compliance method.

The X-ray equipment with a rotating anode was used for the measurement of the austenitic and martensitic phases based on the diffraction in each phase by Cu-Kα. The crystallographic orientaion analysis was performed on the specimen surfaces by

Table 1. Transformation temperatures.

	Martensite transformation finish temperature M_f(℃)	Martensite transformation start temperature M_s(℃)	Reverse transformation start temperature A_s(℃)	Reverse transformation finish temperature A_f(℃)
FML4	−1	21	34	61
FML6	—	-62	—	-20

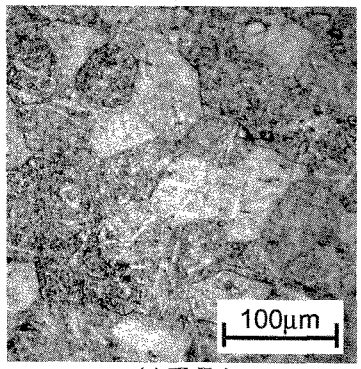

(a) FML4

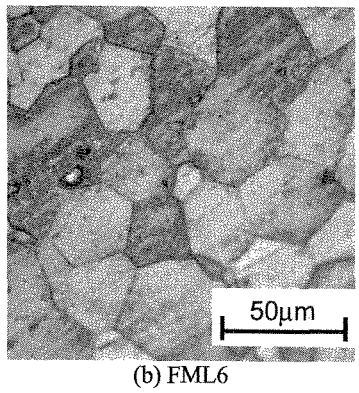

(b) FML6

Fig. 1. Etched specimen surface.

Table 2. Grain size.

	d_L (μm)	d_R (μm)	d_{eq} (μm)
FML4	54.8	46.2	41.4
FML6	28.1	26.4	24.1

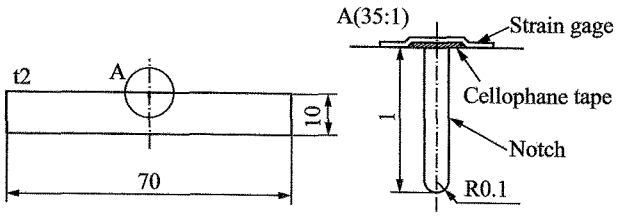

Fig. 2. Single-edge-notched specimen.

EBSP. The lattice parameter of B2 for austenite and B19 for martensite[2] were employed for the analysis.

The stress intensity factor was calculated by the equation below derived from BEM analysis under the condition of the constant displacement applied on the both edges in the axial direction.

$$K=\sigma\sqrt{\pi a}F \quad (1)$$

$$F=1.12-0.419\left(\frac{a}{W}\right)+5.94\left(\frac{a}{W}\right)^2-24.9\left(\frac{a}{W}\right)^3$$
$$+42.6\left(\frac{a}{W}\right)^4-4.87\left(\frac{a}{W}\right)^5+52.2\left(\frac{a}{W}\right)^6-37.3\left(\frac{a}{W}\right)^7 \quad (2)$$

The crack length including the notch length is a and W is the specimen width. The stress intensity range ΔK was defined as the difference between the maximum stress intensity factor K_{max} and minimum stress intensity factor K_{min}.

3. RESULTS AND DISCUSSION

3.1 Characterization of material

The results of tensile tests are presented in Fig. 3 and summarized in Table 3. The symbols σ_T, σ_M, σ_Y, σ_B, E_1 and E_2 denote the transformation stress from austenitic to maratensitic phase, reorientation stress of martensitic phase, yield stress , tensile strength, Young's modulus before σ_T or σ_M and Young's modulus of austenitic phase, respectively. The tensile strength and Young's moduli in the austenitic and martensitic regions are higher in FML6. FML4 possesses

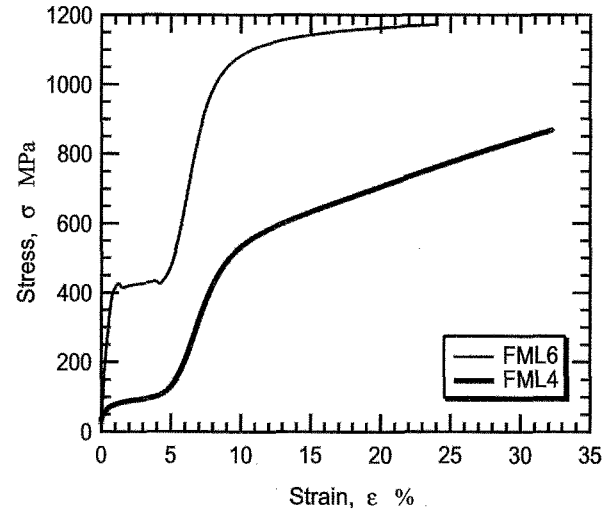

Fig. 3. Result of tensile test.

Table 3. Mechanical properties.

	Transformation or reorientation stress σ_T or σ_M (MPa)	Yield stress σ_Y (MPa)	Tensile strength σ_B (MPa)	Young's modulus E_1 (GPa)	Young's modulus E_2 (GPa)
FML4	65	481	985	26.6	10.9
FML6	285	933	1176	31.6	21.9

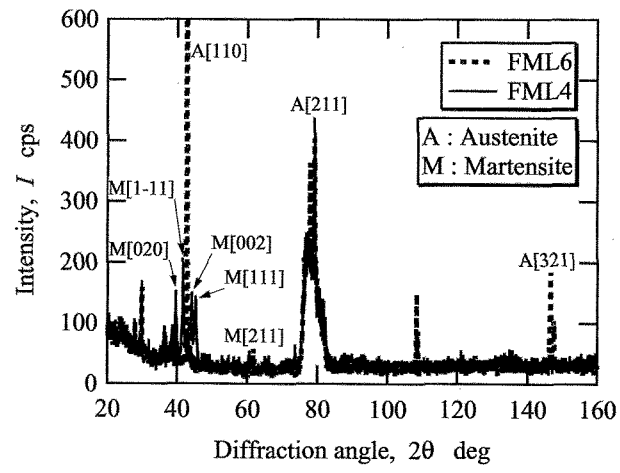

Fig. 4. X-ray diffraction measurement.

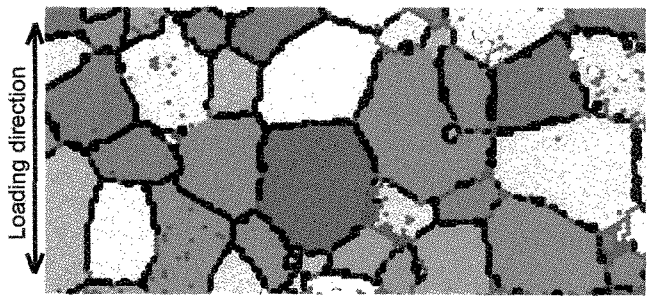

Fig. 5. IPF mapping (Black boundary : high angle grain boundary).

larger elongation at fracture. The result of x-ray diffraction measurement in Fig. 4 shows that FML6 is austenitic, whereas FML4 consists of martensite as well as austenite at room temperature. The crystallographic orientation analysis by EBSP was performed on the specimen surface of FML6 polished by colloidal silica before the fatigue test. Figure 5 shows the inverse pole figure mapping of the surface where the black line indicates the high angle grain boundary with the angle difference of more than 15 degrees. About 90 percent of the grain boundary is the high angle grain boundary.

3.2 Fatigue crack propagation behavior

The relation between crack propagation rate da/dN and stress intensity range ΔK is shown in Fig. 6. When compared at the same ΔK, da/dN in FML4 is lower than that in FML6. In the range more than $da/dN = 1 \times 10^{-9}$ m/cycle, da/dN in FML4 was 1/5 of that in FML6. The difference was remarkable at the threshold, where the threshold stress intensity range ΔK_{th} = 6.6 MPa$\sqrt{m}$ in FML4, whereas ΔK_{th} is 2.7 MPa$\sqrt{m}$ in FML6. The slope of the line fit to the date beyond $da/dN = 1 \times 10^{-9}$ m/cycle based on Paris' law was 3.96 and 4.59 for FML4 and FML6 respectively.

Figure 7 shows the relation between da/dN and effective stress intensity range ΔK_{eff}. Even when da/dN is compared at the same ΔK_{eff}, FML4 exhibited lower crack propagation rate and higher threshold value of ΔK_{eff}. Those results indicate that other factors, such as the difference in the distribution of stress-induced martensite around the crack, are more dominant than crack closure effect.

3.3 Microstructural effect on crack propagation

In order to investigate the effect of microstructure on crack propagation, the specimen surface was observed by scanning electron micrograph and crystallographic orientation analysis by EBSP. Figure 8(a) shows the etched specimen surface of FML6 at ΔK = 9 MPa $\sqrt{m}$. The arrows indicate the cracks arrested at the grain boundaries. The corresponding inverse pole figure mapping is shown in Fig. 8(b). The wireframe images of cubes in (b) represent the orientation of each grain with the lattice of bcc. The high angle grain boundary is white. The crack arrest is observed at the grain boundary between the grains I and II with the angle difference of 39 degrees and between the grain III and IV with the angle difference of 49 degrees. The high angle grain boundaries are considered to operate as the barriers against fatigue crack propagation. Bifurcation of the fatigue crack was found in the grain II and III as well as the grain boundary between V and VI with the angle difference of 59 degrees.

Based on the result of tensile test, FML6 is expected to yield stress induced martensitic phase in the process zone ahead of

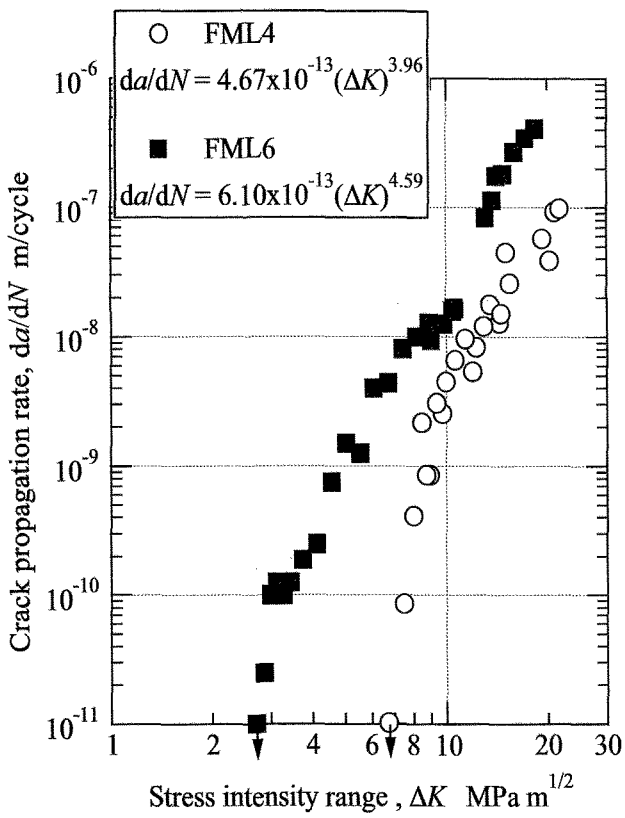

Fig. 6. Relation between da/dN and ΔK.

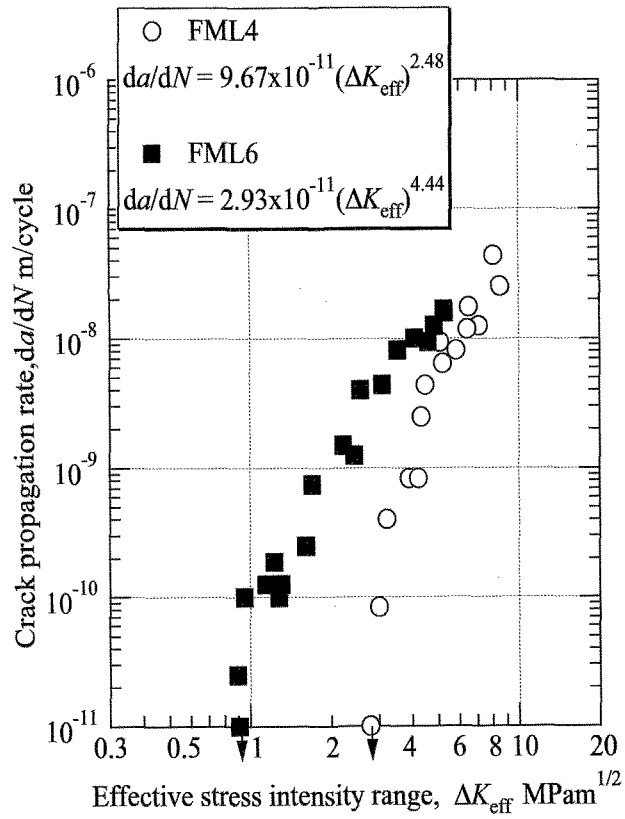

Fig. 7. Relation between da/dN and ΔK_{eff}.

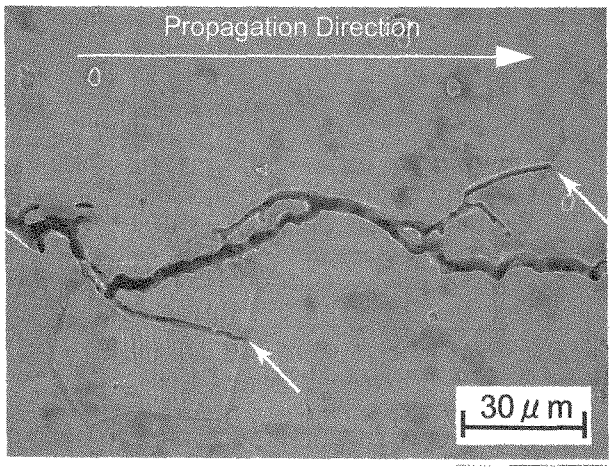

(a) SEM image

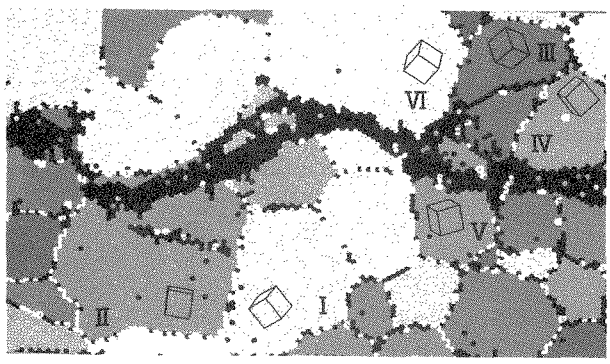

(b) Corresponding IPF image by EBSP

Fig. 8. Specimen surface after fatigue test in FML6.

the crack under cyclic loading. This implies that fatigue crack propagates in the martensitic phase in FML6 in the same way as in FML4, resulting in little difference in the fatigue crack propagation behavior. However, the experimental results showed the remarkable difference as presented in Fig. 6 and 7. The size of the stress induced martensite in FML6 calculated from the equation for plastic zone under plane stress condition with $\sigma_Y = \sigma_M$ is approximately 40 μm at $\Delta K = 9$ MPa$\sqrt{\text{m}}$. In the area within the 40 μm, however, crack tip and crack wake was found to be austenitic and no martensite appeared around the crack based on the crystallographic analysis by EBSP. This result explains the difference in the crack propagation behavior between FML4 and FML6. Even though FML6 yields stress induced martensitic phase under static loading, the mechanism dose not operate under cyclic loading, resulting in the crack propagation in austenitic phase. On the other hand, the crack propagation in FML4 is confirmed to operate in martensitic phase by x-ray diffraction measurement. This difference of phase surrounding the fatigue crack is expected to be the dominant factor to yield the difference in the fatigue crack propagation behavior between FML4 and FML6.

4. CONCLUSION

The fatigue crack propagation behavior of TiNi alloys was studied. The results of shape-memory TiNi and superelastic TiNi were compared and the microstructural effect on the crack propagation behavior was investigated. The results obtained are summarized as follows:

(1) The crystallographic orientation analysis by EBSP showed that about 90 % of the grain boundaries are high angle grain boundary.

(2) The crack propagation rate, when compared at the same stress intensity range, was lower in FML4 than that in FML6. The threshold value of stress intensity range was higher in FML4.

(3) The crack propagation in FML4 is in martensitic phase, whereas that is in austenitic phase in FML6. The difference of phase surrounding the fatigue crack is expected to be the dominant factor to yield the difference in the fatigue crack propagation behavior between FML4 and FML6.

REFERENCES

[1] A. L. McKelvey and R. O. Ritchie, Metall. Mater. Trans. A, 32A, pp. 731-743 (2001)

[2] Y. Kudoh, M. Tokonami, S. Miyazaki and K. Otsuka, Acta Metall. Vol. 33-11, pp. 2049-2056 (1985)

(Received December 21, 2002; Accepted Febuary 14, 2003)